Spatial distribution of αs_1-caseins and β-caseins in milk gels acidified with glucono-δ-lactone

Food Hydrocolloids 139 (2023) 108506

Contents lists available at ScienceDirect

Food Hydrocolloids

journal homepage: www.elsevier.com/locate/foodhyd

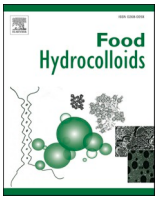

Spatial distribution of αs_1-caseins and β-caseins in milk gels acidified with glucono-δ-lactone

Sanam Foroutanparsa [a], Mariska Brüls [a], C. Elizabeth P. Maljaars [b], Roderick P. Tas [a], Ilja K. Voets [a,*]

[a] Laboratory of Self-Organizing Soft Matter, Department of Chemical Engineering and Chemistry & Institute for Complex Molecular Systems, Eindhoven University of Technology, P.O. Box 513, 5600 MB, Eindhoven, the Netherlands
[b] DSM Biotechnology Center, Alexander Fleminglaan 1, 2613 AX, Delft, the Netherlands

ARTICLE INFO

Keywords:
αs_1-casein
β-Casein
Milk gels
Glucono-δ-lactone
Super-resolution nanoscopy
Stimulated emission depletion (STED)

ABSTRACT

Acid-induced destabilization of casein micelles leads to coagulation of milk which plays an important role in the formation of yogurt. The resulting protein network is formed by aggregation and reconfiguration of casein micelles, including the release of a portion of caseins from these micelles. It is so far unknown how individual αs_1- and β-caseins are organized within this complex network, and how their distribution depends on yogurt composition and processing. Here, we imaged the spatial distribution of caseins using stimulated emission depletion (STED) microscopy and single-molecule localization microscopy (SMLM). We used fluorescently tagged antibodies against αs_1-and β-caseins to localize them inside glucono-δ-lactone (GDL)-acidified milk gels. We conducted quantitative skeleton analysis of STED images and showed that αs_1-and β-caseins contribute with different levels of connectivity to the acid induced milk network.

1. Introduction

Yogurt is made through the acidification of milk by lactic acid bacteria (LAB). LABs produce lactic acid by the fermentation of milk carbohydrates, leading to a drop in pH (Kanauchi, 2019). This process causes destabilization and gelation of casein micelles, which are composed of αs_1-, αs_2-, β-, and κ-caseins at an approximate molar ratio of 4:1:4:1, and constitute 80% of total milk proteins (Walstra, 1990). Whey proteins make up the remaining 20% of milk proteins and contribute to network formation when denatured by heat, modifying both the physical and mechanical properties of the gels (Kalab et al., 1976; Lucey et al., 1997, 2022). The arrangement of and interactions between these milk proteins and LAB metabolites, such as exopolysaccharides, underly the sensory and physical properties of yogurt (Aguilera, 2005).

Electron and fluorescence microscopy visualizations of yogurt network formation and microstructure have shown that milk protein gels are composed of clusters and strands at length scales above tens of μm (Harwalkar & Kalab, 1986; Modler & Kalab, 1983). Moreover, a handful of ensemble studies using nuclear magnetic resonance (NMR) spectroscopy (Sone et al., 2022), spin-echo small angle neutron scattering (SESANS) and rheology measurements of transglutaminase (TGAse)-crosslinked caseins (Nieuwland et al., 2015) have revealed that during milk acidification major rearrangements take place within the casein micelles at the molecular level. These molecular rearrangements and changes in protein conformation and interactions affect the mechanical characteristics of the final gel (Nieuwland et al., 2015). Thus far, it is known that acidification is accompanied by solvation of calcium phosphate within casein micelles (Dalgleish & Law, 1989), collapse of κ-casein brushes on the surface of micelles (De Kruif, 1997) and release of a portion of caseins from the micelles (Dalgleish & Law, 1988). The exact arrangement of the caseins in the milk gels remains elusive due to the limited resolution of conventional light microscopy techniques and challenges in labeling specificity of the individual components. The implementation of new tools capable of mapping out the spatial distribution of distinct proteins in dairy gels at submicron resolution would overcome these shortcomings and help to better understand the mechanisms involved in milk gelation and to elucidate the parameters that influence network microstructure and mechanics.

Super resolution microscopy (SRM) techniques have emerged as powerful tools in life sciences that enable the visualization of complex structures with resolution beyond the classical diffraction limit (Pujals et al., 2019). The application of SRM has recently gained much attention

* Corresponding author.
E-mail address: i.voets@tue.nl (I.K. Voets).

https://doi.org/10.1016/j.foodhyd.2023.108506
Received 30 August 2022; Received in revised form 4 January 2023; Accepted 22 January 2023
Available online 23 January 2023

for characterizing food microstructure as it enables to visualize the spatial arrangement of fluorescently tagged biomacromolecules at nano- and mesoscales (Foroutanparsa et al., 2021; Glover et al., 2019; Hohlbein, 2021). One of these tools is stimulated emission depletion (STED) (Glover et al., 2020; Hell & Wichmann, 1994) microscopy, which uses one laser for excitation and a second, doughnut-shaped depletion laser to limit the area from which light is emitted around the focal point therefore improving the optical resolution to 50 nm and better. This resolution makes STED microscopy well suited to characterize complex food systems since it allows non-invasive measurements of turbid samples with sufficient resolution to resolve nanometric constituents, such as casein micelles in dairy gels.

In this work, we aim to localize αs_1-and β-caseins inside acid-induced milk gels using specific primary antibodies to identify the αs_1-and β-caseins and measure the connectivity of the formed networks. To accomplish this, we use STED microscopy to characterize model gels and yogurt-like dairy gels with high spatial resolution and measure the connectivity of caseins within the network using a semi-automated skeleton analysis (Arganda-Carreras et al., 2010; Doube et al., 2010; Lee, 1994). Furthermore, we validate our STED visualizations using two single-molecule localization microscopy (SMLM) approaches, direct stochastic optical reconstruction microscopy (dSTORM) (Rust et al., 2006) and photo-activated localization microscopy (PALM) (Betzig et al., 2006). Our quantitative SRM imaging approach reveals that β-caseins are present throughout the entire protein network, whereas αs_1-caseins distribute more heterogeneously, especially within the yogurt-like gel. We propose that the observed differences in connectivity of the casein networks are due to a complex interplay between partial disintegration, aggregation and gelation of casein micelles and caseins released from the micelles. We anticipate that the ability to precisely localize individual caseins within complex matrices by STED using casein-specific antibodies will be exploited in future studies on structure-property relations to examine e.g. the impact of changes in various processing steps, such as acidification rate, on the structure and rheological properties of milk protein networks.

2. Materials and methods

2.1. Materials

Milk protein concentrate (MPC80) was kindly provided by the Hungarian Dairy Research Institute Ltd., where it was produced by ultrafiltration and diafiltration of milk, followed by heat treatment (direct steam infusion, 130 °C for 20 s), vacuum evaporation and spray-drying of the resultant retentate. MPC80 composed of 80% milk proteins (with a casein-to-whey protein ratio of 80:20), 7.5% ash, 5.5% lactose, 5% water. Low-fat milk (Dutch: half volle melk) was purchased from local supermarket. Poly-L-lysine (Cat. No. P8920), phosphate buffer tablets (Cat. No. P4417), ATTO647N–NHS ester dye (Cat. No. 94822) were purchased from Sigma-Aldrich, Merck Life Science NV, The Netherlands. Paraformaldehyde 32% Aqueous SOL. EM GRADE (Cat. No.15714) was purchased from Electron Microscopy sciences, Hatfield, U.S.A. D-(+)-gluconic acid δ-lactone (GDL, ≥99.0%, Cat. No. A13105) was purchased from Alfa Aesar, Thermo Fisher Scientific, Kandel, Germany. Rabbit anti-bovine β-casein polyclonal antibody (Cat. No. BS-10032R) and rabbit anti-bovine αs_1-casein polyclonal antibody (Cat. No. BS-10033R) were obtained from Bioss Inc., Ferienigde State, U.S.A. Amicon Ultra-0.5 Centrifugal Filter Unit (10 000 Da molecular weight cut off, Cat. No. UFC501024) were obtained from Merk Millipore, the Netherlands. Zeba Spin Desalting Columns (7K MWCO, Cat. No. 89882) were purchased from Thermo Scientific™, The Netherlands.

2.2. Preparation of GDL-induced milk gels

Solutions of milk protein concentrate (MPC80) and low-fat milk were used as milk medium. The different gels were prepared upon acidification of non-heated 11% MPC80, non-heated 4.5% MPC80, heated 4.5% MPC80, and heated low-fat milk, in the following manner. First, 11 wt% MPC80 was reconstituted in Milli-Q water, shaken for 1 h, and stored overnight at 4 °C to become hydrated. For nonheated 11 wt% MPC80 gel, the 11 wt% MPC80 solution was acidified by adding 2 wt% D-(+)-gluconic acid-δ-lactone (GDL). For nonheated 4.5 wt% MPC80, 11 wt% MPC80 was first diluted to 4.5 wt% and then acidified by adding 1.5 wt% GDL. For heated 4.5 wt% MPC80, the 4.5 wt% MPC80 solution was heat treated in a thermomixer (Eppendorf® ThermoMixer® C, Homburg, Germany) for 30 min at 90 °C and 15 min at 85 °C with gentle agitation (300 rpm). After cooling to room temperature (RT), the solution was acidified with 1.5 wt% GDL. For the yogurt-like gel, the low-fat milk was heat treated according to the above procedure and then acidified with 1.5 wt% GDL. The GDL concentration was adjusted so that the final pH for all model systems was 4.3 ± 0.2 over 6–7 h of incubation at RT. Therefore, a slightly higher GDL concentration was used for acidification of reconstituted 11% MPC80, which had a higher pH (pH ∼ 7) compared to natural milk. After addition of GDL, all model systems were incubated overnight at RT, after which samples were prepared for imaging as described below.

2.3. CSLM/STED microscopy of model dairy gels

2.3.1. Immobilizing and labeling acid milk gels

To immobilize acid milk gels onto the surface via electrostatic interactions, cationic poly-L-lysine (PLL) was applied to coat the surface. Cover slides were first cleaned with isopropanol and then coated with PLL and then washed thoroughly with Milli-Q as described in (Foroutanparsa et al., 2021). Afterwards a small piece of milk gel sample was carefully transferred on the microscope slide taped with two strips of double-sided adhesive tape and PLL-coated coverslip was placed on top to make a flow chamber containing a turbid acid milk gel. Sample was incubated inside the chamber upside down at RT for 10 min. Thereafter, for subsequent fixation, 25 μl of 4% (w/v) freshly prepared formaldehyde solution in 10 mM phosphate buffer solution (PBS) was injected in the chamber and incubated upside down at RT for 20 min (Jimenez et al., 2020). Subsequently, the chamber was rinsed by injecting 3 times 200 μl of PBS inside to make it ready for staining. To localize β- and αs_1-casein using STED, rabbit anti-bovine β-casein polyclonal antibody or rabbit anti-bovine αs_1-casein polyclonal antibody were directly labeled with ATTO647N–NHS ester dye, which is a suitable dye for Stimulate emission depletion (STED) microscopy, using protocol described (Berg & Fishman, 2019). Briefly, prior to labeling, antibodies were filtered to remove Glycerol using Amicon Ultra-0.5 centrifugal filter units (10 000 Da molecular weight cut off) or Zeba Spin Desalting Columns (7K MWCO). Labeling reaction was performed in carbonate buffer (pH 8.5) overnight at 4 °C, and free dyes were removed from the solution using centrifugal filters. Final antibody concentration and degree of labeling were determined by spectrophotometric analysis using a NanoDrop spectrophotometer (Thermo Fisher Scientific, the Netherlands). The degree of labeling of antibodies was calculated to 2.5–4.5 mol of dye per mole of antibody. The dye-conjugated primary antibodies were used within 3 days after labeling. For staining, they were diluted to 200 μg/ml and 25 μl of each was injected into the microscopy chambers containing acid milk gel from the same batch and incubated at 4 °C overnight. Following extensive washing with PBS buffer, the chamber was sealed ready for STED microscopy.

2.3.2. CSLM/STED microscopy

Imaging was performed using a STED microscope (Abberior Instrument, Göttingen, Germany) equipped with UPlanSApo 100x/1,40 Oil [infinity]/0,17/FN26,5 objective (Olympus), a Katana-08 HP laser (Onefive) and multiple laser lines at 405 nm, 488 nm, 561 nm, 640 nm, and the pulsed laser at 595 nm and 775 nm (power = 3 W); plus Imspector 0.14.13 919 software. Typically, the images were acquired with pixel size of 30 nm, and a pixel dwell time of 10 μs. Images were

taken at different locations on each coverslip, and 1–2 μm above the coverslip where the structure was fixed and immobilized with the highest signal to noise ratio. A pinhole was set at 1.00 AU at 100x. ATTO647N dye was excited at 640 nm (5% laser power), whereas STED was achieved using a wavelength of 775 nm (4% laser power equal to 120 mW).

2.3.3. Image analysis of STED images: skeleton analysis

A skeleton analysis method was used to quantify caseins (β- and αs_1-caseins) topology in yogurt gel. All the analysis steps were performed using Fiji/Image J software (https://imagej.net/software/fiji/) (Schneider et al., 2012). For skeleton analysis, first 8-bit STED TIFF images were noise reduced by applying Gaussian filter (radius = 2) and then binarized using the mean grey level as threshold. The resulting binarized images of protein domains were skeletonized (Fiji, skeleton plugin) to produce one-pixel wide representative image (Lee, 1994). Furthermore, the skeletonized images comprising a network of branches were analyzed by AnalyzeSkeleton plugin (Arganda-Carreras et al., 2010). AnalyzeSkeleton classifies the pixels within the thinned protein domains based on their 26 neighboring positions into three categories: end-points pixels, which have less than 2 neighbors, junction pixels with more than 2 neighbors and slab pixels which have exactly 2 neighbors. Slab pixels are building blocks of branches that connect end and junction points. Additionally, the possible loops were pruned by cutting the loop branches from its darkest pixel by choosing "lowest intensity voxel" as prune cycle method.

2.3.4. Measuring connectivity

To define the connectivity of skeleton, we aimed to identify dangling ends and loop defects within the network. Dangling ends, branches connecting to the end points were eliminated by choosing "Prune Ends" option of the plugin. Branches with Euclidean distance of less than 100 nm (about the resolution of STED microscopy) were termed as dangling loops and further removed. Therefore, link density, a metric to assess the connectivity, was obtained for individual images from a ratio of total number of linking branches excluding dangling ends and loops to total number of branches. In addition, AnalyzeSkeleton provides information on total length of branches per skeletons, skeleton length, identified in the field of view. To compare the skeleton lengths detected at each condition, we provided the length-weighted frequency of skeleton length of seven size categories. For each condition, the length-weighted frequency of skeleton length was achieved by multiplying the relative frequency of a skeleton length by its corresponding length and dividing the result to the average skeleton length. Then for simplifying the graph, the length-weighted frequency of given skeleton length was classified by interval of 100 μm and normalized by sum.

2.4. Statistical methods

Normality tests were performed using a Shapiro-wilk test and Normal Q-Q plot which showed that link density distribution was not normal at all conditions. Therefore, the statistical difference in link density distributions of, total protein network, αs_1-and β-caseins in GDL-acidified gel of nonheated 11 wt% MPC80 and heated low-fat milk, and αs_1-and β-caseins in GDL-acidified gel of nonheated and heated 4.5 wt% MPC80 were compared pairwise with non-parametric one-way ANOVA tests (Kruskall-Wallis). All the statistical analyses were performed using IBM SPSS statistics Version 25.0 software and results with a P-value <0.05 were considered statistically significant.

3. Results and discussion

3.1. Sub-micron localization of αs_1-and β-caseins in GDL-acidified model and yogurt-like dairy gels

Model gels and yogurt-like dairy gels with different composition and heat treatment were prepared by glucono-δ-lactone (GDL)-induced acidification of reconstituted milk protein concentrate (MPC80 containing 80% milk proteins and no fat) for model gels, or low-fat milk for yogurt-like gels. Model gels with MPC80 were prepared at either a high protein content (11% w/v) or low protein content (4.5% w/v). Yogurt-like gels were prepared from low-fat milk containing 3.5% milk proteins and 1.5% fat. The heat-treated yogurt-like gel and the low-protein model gels were heated as in yogurt production to denature the whey protein fraction prior to acidification. All gels were mounted on a coverslip, fixated by formaldehyde, and subsequently stained with ATTO647N-labeled antibodies specific to αs_1-and β-casein for STED imaging. We also stained the entire protein network, consisting of 80% caseins and 20% whey proteins, in the simplest model gel (nonheated 11% (w/v) MPC80) and in the yogurt-like gel, with the amine-reactive ATTO647N–NHS ester (A647N). With this approach, we aim to map out the distribution of the two types of caseins and assess if this is affected by the milk protein content, presence of fat, and heating or not.

We first tested whether the antibodies showed binding to other macromolecules present in the dairy gels, such as β-lactoglobulin, and confirmed their specificity by STED imaging of the control samples (see materials and method, and Supplementary Fig. S1). Subsequently, the nonheated and heated gels were imaged simultaneously by STED microscopy and confocal laser scanning microscopy (CLSM) to assess how well the labeled components could be resolved within all gels (Fig. 1). Diffraction-limited CLSM images of the dairy gels did not show marked differences in casein distribution and network architecture (Fig. 1, the top half of zoomed-out images). Both caseins appeared to generate a connected structure with microscale variations in brightness, which seem slightly more pronounced in the heated yogurt-like gel. To take a closer look at the casein distribution and gel structure at smaller length scales, we turned to STED microscopy (Fig. 1, the bottom half of zoomed-out images). STED offered about a two-fold increase in resolution (see Supplementary Fig. S2) revealing clear differences in domain structure and spacing between the gels (Fig. 1, the zoomed-in images). In the simplest model system, nonheated 11% (w/v) MPC80 (NH 11% MPC80), β-caseins appeared to form an interconnected network, while αs_1-casein (mostly) accumulated more heterogeneously, partially in the form of distinct spherical structures spaced apart by rather large distances (Fig. 1A). These trends were also observed with fewer details in dual-color CLSM images of NH 11% MPC80 that showed a dense network of β-casein and a heterogenous distribution of αs_1-casein all around the β-caseins network (see Supplementary Fig. S3). Next, we examined whether the distribution of the two caseins changed upon a reduction in the protein concentration in the model system to a similarly low protein concentration as in milk. In nonheated 4.5% (w/v) MPC80 (NH 4.5% MPC80), αs_1-casein domains appeared less connected compared to the β-casein network. Both the αs_1- and β-casein structures appeared less dense than those in the model gels with a higher protein content (NH 11% MPC80) (Fig. 1B). Heating 4.5% (w/v) MPC80 resulted in the formation of a dense and compact network of β-caseins, and a fine network of αs_1-caseins with some domains of higher concentrations (Fig. 1C). A similarly compact β-casein network was also observed in the yogurt-like gel, which was obtained by heating low fat milk (Fig. 1D). By contrast, αs_1-caseins did not adopt such a compact network-like architecture in the yogurt-like gel. Instead, the αs_1-casein network looks rather coarse, comprising of seemingly loosely-connected domains. In sum, in all model gels we observed a highly-interconnected network of β-caseins which densifies upon heat-treating the milk protein source. αs_1-caseins accumulated in less-connected domains compared to β-caseins across all samples. In heated 4.5% MPC80 gels, the αs_1-casein domains appeared more connected than in the other gels. Single-color dSTORM and two-color SMLM microscopy of the simple model gel (NH 11% MPC80) and yogurt-like system (H LFM) agreed with the corresponding STED images and showed the same trend in the distribution of the two caseins (see Supplementary Figs. S4–6). Having visualized the arrangement of caseins within different dairy gels with

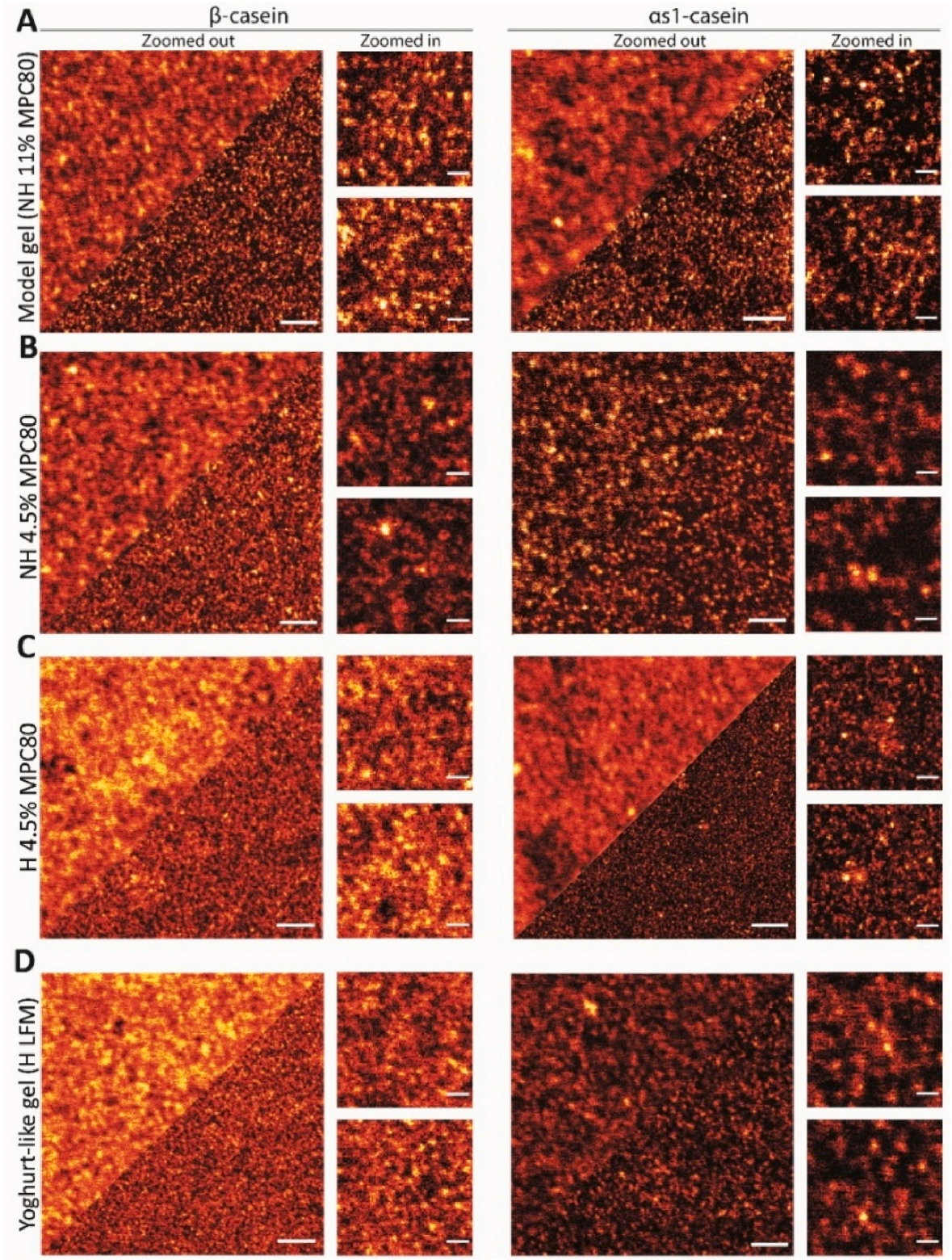

Fig. 1. STED imaging of the arrangement of αs_1**- and β-caseins in GDL-induced milk gels (with final** pH **4.3 ± 0.2) of: (A)** 11% (w/v) reconstituted (nonheated) MPC80 solution (NH 11% MPC80). **(B)** 4.5% (w/v) reconstituted (nonheated) MPC80 solution (NH 4.5% MPC80). **(C)** 4.5% (w/v) reconstituted (heated) MPC80 solution (H 4.5% MPC80). **(D)** (heated) low-fat milk (H LFM). In A-D panels, the left panels display β-caseins distribution in confocal (top) and STED (bottom) images. The right panels display αs_1-caseins distribution in confocal (top) and STED (bottom) images. Scale bars represent 2000 nm in zoomed-out images, and 500 nm in zoomed-in images.

submicron precision, we next set out to quantitatively analyze the observed differences in the STED images acquired for the two models with the largest compositional differences. Therefore, for further characterization, we selected the images of nonheated model gels with high milk protein content and no fat (NH 11% MPC80) and heated yogurt-like gels with low protein content and 1.5% fat (H LFM).

3.2. αs_1-caseins and β-caseins contribute to the acid-induced protein network with different levels of connectivity

We employed skeleton analysis to study the connectivity of the αs_1- and β-casein domains within the food networks visualized by STED (Arganda-Carreras et al., 2010; Doube et al., 2010). For this purpose, STED images were first binarized (Fig. 2A–B), after which the binarized protein domains were thinned to produce a skeleton of the network (Fig. 2C, and Supplementary Figs. S7–10). The skeletonized images were then further analyzed using the Analyze Skeleton ImageJ plugin (Arganda-Carreras et al., 2010; Doube et al., 2010) to obtain the number of branches, corresponding to the lines that connect the junctions within the skeleton (black in Fig. 2D). We divided the branches into three types: dangling ends connected to the endpoints (as shown by the arrow in Fig. 2D and which are removed in Fig. 2E), dangling loops (two branches that end-up in the same junction), and linking branches, being all other branches, which are not identified as dangling ends or dangling loops. Therefore, we obtained the link density of each image from the ratio of the total number of linking branches (excluding dangling ends and loops) to the total number of branches in the same image (which includes dangling ends and loops) (Fig. 3). The link density was used to characterize the connectivity of the network formed by αs_1-and β-caseins represented in the two-dimensional (2D) images. Note that the link density which we compute in this manner *reflects* network connectivity, but it will deviate from theoretical values for (ideal) three-dimensional polymer gels, because aggregates and finite clusters are not excluded from the analysis and because we analyze a 2D projection of a 3D network.

To characterize the connectivity of the whole protein network and the αs_1-and β-casein networks in the model gels and the yogurt-like gels, we performed skeleton analysis of STED images acquired from networks stained with amine-reactive ATTO647N–NHS ester (A647N), or the αs_1- and β-casein antibodies (Fig. 3A). Analysis showed an interconnected porous structure with an average link density of 0.6 for both the model gel and the yogurt-like gel when stained nonspecifically with ATTO647N dye (Fig. 3B). The maximal link density of 0.6 is lower than the theoretical value of 1 for a fully connected network without dangling ends and loop defects (Grillet, Anne, Nicholas, & Lindsey, 2012). In such ideal, end-linked polymer gels, all branches are connected via junctions. We tentatively attribute the lower link density to the architecture of the network (which is not an ideal, end-linked polymer gel, but does contain dangling ends and loops) and to the analysis scheme which is based on a 2D image of a 3D gel. Connectivity measurements performed on milk protein networks in which either αs_1-or β-caseins were localized using primary antibodies suggest differences in the connectivity of αs_1-caseins and β-caseins. Both qualitative assessment and quantitative connectivity measurements showed a clear difference in the link density distribution of αs_1-and β-caseins in both gels. Average link densities of β-caseins in model gels and yogurt-like gels were 0.5 ± 0.08 and 0.6 ± 0.02, respectively and did not differ significantly from each other. In both cases, αs_1-casein connectivity was much lower with link densities of 0.39 ± 0.14 and 0.34 ± 0.06 (Fig. 3B). A skeleton analysis on the other model gels (Fig. 3C) showed that the αs_1-casein network link density is lower than the β-casein link density regardless of the protein composition and heat treatment of the model dairy gels. The difference in αs_1-casein and β-casein link density is most pronounced (and significant according to statistical analysis) for the yogurt-like gel. This is probably due to the compositional differences between the yogurt-like gel compared to the other gels, such as the presence of heat-denatured whey proteins, heat-treated fat globules (Sharma & Dalgleish, 1993), and/or differences in ionic strength and mineral content (Famelart et al., 1996; Reitmaier et al., 2020).

To further characterize the network formed by the two caseins, we compare the total length of branches within the skeletons (including dangling ends and loops) (Fig. 4A), for which we introduce the term skeleton length (Fig. 4). Skeleton length is the total length of branches within skeletons (connected structures in the field of view). The skeleton length distributions obtained from images of the model gel (Fig. 4B) and the yogurt-like gel (Fig. 4C) subjected to nonspecific and β-casein staining were similar and enriched in skeleton lengths greater than 300 μm. By contrast, the same skeleton analysis of images of gels in which the αs_1-casein domains were stained yielded different skeleton length distributions skewed toward smaller values, with the majority of skeleton lengths below 100 μm. Thus, both the link densities and skeleton length distributions indicate that αs_1-caseins are more heterogeneously localized than β-caseins within the model gel and yogurt-like gel. We also note that the skeleton lengths of the yogurt-like gels (stained aspecifically or with the β-casein antibody) were somewhat longer than the corresponding skeleton lengths of the model gels, suggesting a finer network architecture, as shown schematically in Fig. 4A.

3.3. Role of αs_1-caseins and β-caseins in the formation of GDL-acidified dairy gels

Based on the STED images and our quantitative analysis of the

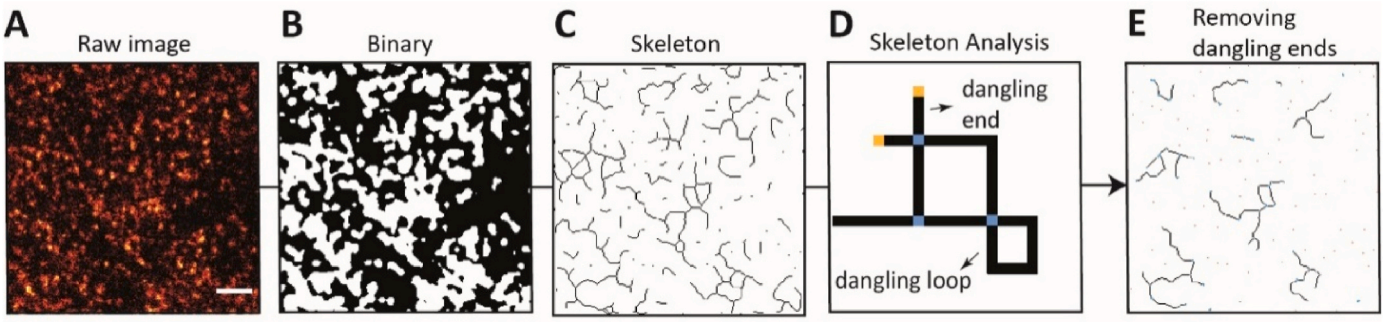

Fig. 2. Connectivity of the GDL-induced casein network measured by skeleton analysis of STED images. Processing steps prior to skeleton analysis of STED images. (A) Raw STED images. (B) STED images were binarized using a mean grey value of the image as threshold, (C) The binarized domains were thinned to produce skeleton of the network. (D) Skeleton analysis was performed by ImageJ Analyze Skeleton plugin (http://imagej.net/AnalyzeSkeleton) (Arganda-Carreras et al., 2010) to classify pixels within the skeleton and tag branches as black, end points as yellow, and junction points as blue. End point-connected branches are called dangling ends and branches with Euclidean distance of less than 100 nm are called dangling loops. (E) Dangling ends were removed by the "prune end" function in the plugin. Scale bar in panel A is 1 μm.

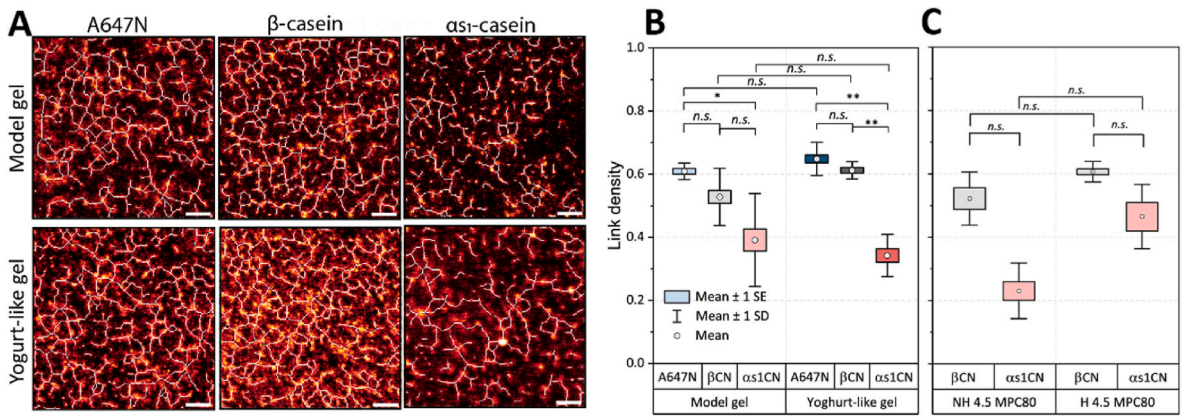

Fig. 3. Connectivity analysis on ATTO647N-, αs_1-and β-caseins-stained model gel and yogurt-like gel. (A) overlay of raw STED images and skeletonized images of network structure in model gel and yogurt-like gel stained with ATTO 647N (A647N), antibodies specific to αs_1-and β-caseins. Scale bars in all images are 1 μm. **(B)** Link density of the entire network, αs_1-caseins and β-caseins structures in STED images of model gel and yogurt-like gel. **(C)** Link density of αs_1-and β-caseins in STED images of NH 4.5% MPC80, H 4.5% MPC80. Notes:**Highly statistically significant at P-value <0.005; * Statistically significant at P- value < 0.05; n.s.: not statistically significant at P-value >0.05.

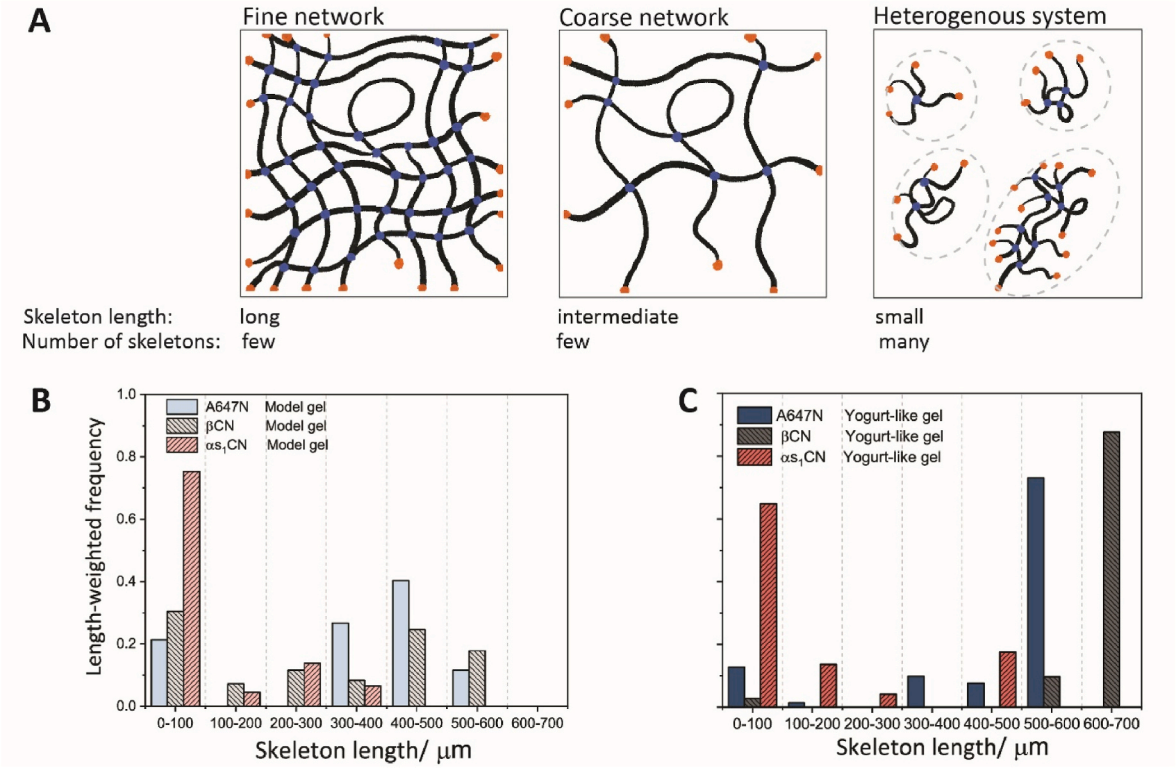

Fig. 4. Characterization of the skeletons. (A) Characterization of the skeletons. (A) Schematic representation (from left to right) of a fine and coarse space-spanning network and a heterogeneous system consisting of smaller disconnected clusters. Branches within the dotted area belong to one skeleton, and total length of branches per skeleton (skeleton length) and the number of skeletons that are expected in the fine and coarse networks and in the heterogeneous system are shown below the schematics. **(B–C)** Length-weighted distribution of skeleton length for: Model gel **(B)** and yogurt-like gel **(C)**.

distribution of αs_1-and β-caseins within the studied milk protein networks, we propose that the final microstructure of the GDL-acidified, nonheated dairy gels develops in the following manner (Fig. 5). During acidification to pH 5.5, casein micelles reconfigure and release both calcium phosphates and a moderate fraction of all casein types (Fig. 5B) (Dalgleish & Law, 1988; Famelart et al., 1996). Release of β-caseins occurs to a larger extent compared to αs_1-casein release (Dalgleish & Law, 1988). As a result, partially disintegrated casein micelles, to which we refer as non-native micellar caseins, remain in solution at pH 5.5 (Fig. 5B) (Ingham et al., 2016; Marchin et al., 2007). The solubility of released caseins, specifically of the calcium-sensitive αs_1-caseins (Post et al., 2012),as well as non-native micellar caseins, deteriorates upon further acidification to pH 5.2 and induces the formation of sparsely-connected aggregates of αs_1-caseins (Fig. 5C) (Bingham, 1971; Dalgleish & Law, 1988). Eventually, acidification to pH values below 4.6 (i.e., below the isoelectric point of the caseins), also compromises the solubility of the other released caseins (mostly β-caseins) to such an extent that these now also aggregate and deposit onto the already present non-native micelles and αs_1-casein domains (Fig. 5D). This generates a more interconnected milk protein network comprising non-native

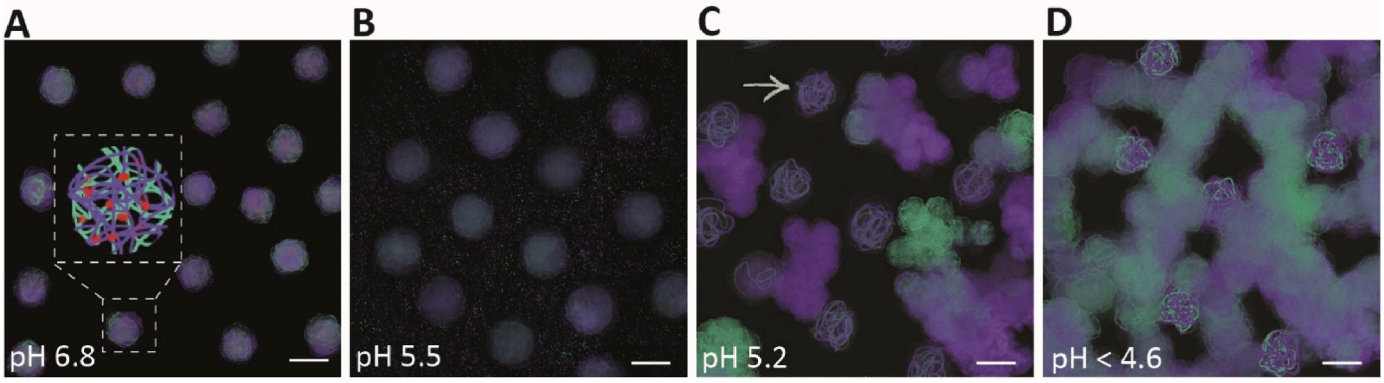

Fig. 5. Schematic representation of the role of αs_1- and β-caseins in the formation of GDL-acidified (nonheated) milk gels.
(A) Casein micelles are sterically stabilized at pH 6.8 (purple: αs_1-casein, green: β-casein, red: calcium phosphate nanoclusters (CaP)). **(B)** At pH ~ 5.5, CaP are dissolved, and caseins (mainly β-and κ-caseins) release from the micelles, leaving behind non-native micellar caseins. **(C)** At pH 5.2, the onset of aggregation, small aggregates form as a result of electrostatic interactions between insoluble αs_1-casein structures and β-caseins. Non-native micellar caseins (indicated by arrow) become insoluble. **(D)** At pH values below 4.6, hydrophobic interactions promote the formation of a network of interconnected β-caseins and loosely entangled αs_1-casein. Scale bars are 200 nm.

micelles and compact, loosely connected αs_1-casein domains which are decorated, interspersed and interconnected by β-casein domains. A similar sequence of events likely takes place in the heat-treated model and yogurt-like gels albeit somewhat differently presumably due to the presence of heat-denatured whey proteins and fat (Ong et al., 2010; Singh et al., 1996). In model gels prepared from heat-treated milk media, heat-denatured whey proteins can interact with and bind to casein micelles (Algleish, 2007, Anema and Li, 2003), limiting the dissociation and disintegration of caseins from micelles at pH of about 5.5 (Heertje et al., 1985; Singh et al., 1996). Consequently, the network might exhibit greater colocalization of αs_1-caseins and β-caseins, which is reflected in our results with a more comparable connectivity of caseins (H 4.5 MPC80 in Fig. 3C). In a yogurt-like gel, it is possible that heat-denatured whey proteins cover the fat droplets (Sharma & Dalgleish, 1993) rather than hindering the dissociation of caseins, and a higher ionic strength and mineral content may lead to a slightly increased release of caseins (Famelart et al., 1996). This could allow for greater dissociation of β-casein from casein micelles at pH 5.5 (Fig. 5B) and consequently a more heterogeneous distribution of αs_1-casein in the final gel forms at pH below 4.6 according to the scenario proposed above. However, in-depth time-resolved studies are required to fully decipher the exact formation mechanism. In this light, it would be helpful to also specifically localize the fat globules and heat-denatured whey proteins within the network and to determine e.g. whether or not they interact with αs_1-caseins and β-caseins.

4. Conclusion

In this work, we used various super-resolution microscopy tools, including stimulated emission depletion (STED) microscopy, and specific labeling of αs_1-caseins and β-caseins to localize αs_1 and β-casein domains within acid milk gels and to examine whether or not the caseins are similarly distributed throughout the protein network. Regardless of the microscopy technique used, we observed differences in the distribution of αs_1-caseins and β-caseins in glucono-δ-lactone(GDL)-acidified milk gels. STED allowed for imaging of the turbid model yogurts at twice the resolution of confocal microscopy, which was helpful for further quantitative analysis of the network architecture. Interestingly, whereas β-caseins are distributed throughout the entire gel, αs_1-caseins distribute more heterogeneously in acid milk gels. This differential distribution was quantified by measuring the connectivity of the two caseins using a skeleton analysis. We attribute the differences in αs_1-and β-casein distribution and domain connectivity to a reorganization of αs_1-and β-caseins in the pH range of 6.8 to 4.6 during GDL-induced gelation as proposed earlier (Heertje et al., 1985). Regardless of protein content or the presence of whey proteins and fat, αs_1-casein domains were less connected compared to β-casein domains. Within a skeleton analysis, this was borne out by a lower link density and a higher fraction of short skeleton lengths in the skeleton length distributions. In the future, it would be of the great interest to investigate how the connectivity of caseins changes in real yogurt fermented with different bacterial strains under physiological conditions, and to examine how the observed microstructures relate to the rheological properties and quality characteristics of the yogurt.

Author statement

Sanam Foroutanparsa: Conceptualization, Investigation and validation, Visualization, Data curation, Formal analysis, Writing - Original Draft.

Mariska Brüls: Conceptualization, Methodology, Writing - Review & Editing.

C. Elizabeth P. Maljaars: Conceptualization, Writing - Review & Editing.

Roderick P. Tas: Conceptualization, Methodology, Writing - Review & Editing.

Ilja K. Voets: Supervision, Funding acquisition, Conceptualization, Writing - Review & Editing.

Declaration of competing interest

All authors declare that they have no conflicts of interest.

Data availability

Data will be made available on request.

Acknowledgment

The authors would like to thank Dr. Maurien Olsthoorn, Dr. Johannes Hohlbein, Dr. Antonio Aloi and Dr. Taco Nicolai for helpful comments and constructive feedback. This publication is part of the project Localbiofood (with project number 731.017.204) of the research program Science PPP Fund, which is (partly) financed by the Dutch Research Council (NWO) in collaboration with ChemistryNL. We would like to thank all our colleagues in the LocalBioFood consortium for valuable discussions.

Appendix A. Supplementary data

Supplementary data to this article can be found online at https://doi.org/10.1016/j.foodhyd.2023.108506.

References

Aguilera, J. M. (2005). Why food micro structure? *Journal of Food Engineering, 67*(1–2), 3–11. https://doi.org/10.1016/j.jfoodeng.2004.05.050

Algleish, D. O. G. D. (2007). *Acid gelation in heated and unheated milks: Interactions between serum protein complexes and the surfaces of casein micelles*.

Anema, S. G., & Li, Y. (2003). Association of denatured whey proteins with casein micelles in heated reconstituted skim milk and its effect on casein micelle size. *Journal of Dairy Research, 70*(1), 73–83. https://doi.org/10.1017/S0022029902005903

Arganda-Carreras, I., Fernández-González, R., Muñoz-Barrutia, A., & Ortiz-De-Solorzano, C. (2010). 3D reconstruction of histological sections: Application to mammary gland tissue. *Microscopy Research and Technique, 73*(11), 1019–1029. https://doi.org/10.1002/jemt.20829

Berg, E. A., & Fishman, J. B. (2019). *Labeling antibodies using N -hydroxysuccinimide (NHS) -fluorescein*. https://doi.org/10.1101/pdb.prot099283, 229–231.

Betzig, E., Patterson, G. H., Sougrat, R., Lindwasser, O. W., Olenych, S., Bonifacino, J. S., Davidson, M. W., Lippincott-Schwartz, J., & Hess, H. F. (2006). Imaging intracellular fluorescent proteins at nanometer resolution. *Science, 313*(5793), 1642–1645. https://doi.org/10.1126/science.1127344

Bingham, E. W. (1971). Influence of Temperature and pH on the Solubility of sl-, and k-Casein. *Journal of Dairy Science, 54*(7), 1077–1080. https://doi.org/10.3168/jds.S0022-0302(71)85974-X

Dalgleish, D. G., & Law, A. J. R. (1988). pH-Induced dissociation of bovine casein micelles. I. Analysis of liberated caseins. *Journal of Dairy Research, 55*(4), 529–538. https://doi.org/10.1017/S0022029900033306

Dalgleish, D. G., & Law, A. J. R. (1989). pH-Induced dissociation of bovine casein micelles II. Mineral solubilization and its relation to casein release. *Journal of Dairy Research, 56*(5), 727–735. https://doi.org/10.1017/S0022029900029290

De Kruif, C. G. (1997). Skim milk acidification. *Journal of Colloid and Interface Science, 185*(1), 19–25. https://doi.org/10.1006/jcis.1996.4548

Doube, M., Klosowski, M. M., Arganda-Carreras, I., Cordelières, F. P., Dougherty, R. P., Jackson, J. S., Schmid, B., Hutchinson, J. R., & Shefelbine, S. J. (2010). BoneJ: Free and extensible bone image analysis in ImageJ. *Bone, 47*(6), 1076–1079. https://doi.org/10.1016/j.bone.2010.08.023

Famelart, M., Lepesant, F., Gaucheron, F., Graet, Y. Le, Schuck, P., Famelart, M., Lepesant, F., Gaucheron, F., Graet, Y. Le, & Schuck, P. (1996). *pH-Induced physicochemical modifications of native phosphocaseinate suspensions : Influence of aqueous phase*.

Foroutanparsa, S., Brüls, M., Tas, R. P., Maljaars, C. E. P., & Voets, I. K. (2021). Super resolution microscopy imaging of pH induced changes in the microstructure of casein micelles. *Food Structure, 30*(January), Article 100231. https://doi.org/10.1016/j.foostr.2021.100231

Grillet, Anne, M., Nicholas, B., Wyatt, & Lindsey, M. Gloe (2012). Polymer gel rheology and adhesion. *Rheology, 3*, 59–80.

Glover, Z. J., Ersch, C., Andersen, U., Holmes, M. J., Povey, M. J., Brewer, J. R., & Simonsen, A. C. (2019). Super-resolution microscopy and empirically validated autocorrelation image analysis discriminates microstructures of dairy derived gels. *Food Hydrocolloids, 90*, 62–71. https://doi.org/10.1016/j.foodhyd.2018.12.004

Glover, Z. J., Francis, M. J., Anne, H., Andersen, U., Buhelt, L., Povey, M. J., Holmes, M. J., Brewer, J. R., & Cohen, A. (2020). Dynamic moisture loss explored through quantitative super-resolution microscopy. *Spatial Micro-viscosity and Macroscopic Analyses in Acid Milk Gels, 101*. https://doi.org/10.1016/j.foodhyd.2019.105501. November 2019.

Harwalkar, V. R., & Kalab, M. (1986). Relationship between microstructure and susceptibility to syneresis in yoghurt made from reconstituted nonfat dry milk. *Food Microstructure, 5*(2), 287–294.

Heertje, I., Visser, J., & Smits, P. (1985). Structure Formation in acid milk gels. *Food Structure Food Structure FOOD MICROSTRUCTURE, 4*(4), 267–277. http://digitalcommons.usu.edu/foodmicrostructure%5Cnhttp://digitalcommons.usu.edu/foodmicrostructure/vol4/iss2/10.

Hell, S. W., & Wichmann, J. (1994). Breaking the diffraction resolution limit by stimulated emission: Stimulated-emission-depletion fluorescence microscopy. *Optics Letters, 19*(11), 780. https://doi.org/10.1364/ol.19.000780

Hohlbein, J. (2021). Single-molecule localization microscopy as an emerging tool to probe multiscale food structures. *Food Structure, 30*(October), Article 100236. https://doi.org/10.1016/j.foostr.2021.100236

Ingham, B., Smialowska, A., Erlangga, G. D., Matia-Merino, L., Kirby, N. M., Wang, C., Haverkamp, R. G., & Carr, A. J. (2016). Revisiting the interpretation of casein micelle SAXS data. *Soft Matter, 12*(33), 6937–6953. https://doi.org/10.1039/c6sm01091a

Jimenez, A., Friedl, K., & Leterrier, C. (2020). About samples, giving examples: Optimized single molecule localization microscopy. *Methods, 174*(May 2019), 100–114. https://doi.org/10.1016/j.ymeth.2019.05.008

Kalab, M., Emmons, D. B., & Sargant, A. G. (1976). Milk gel structure V. Microstructure of yoghurt as related to the heating of milk. *Milchwissenschaft-Milk Science International, 31*(7), 402–407.

Kanauchi, M. (2019). *Lactic acid bacteria: Methods and protocols* (Vol. 1887). http://www.springer.com/series/7651%0Ahttp://link.springer.com/10.1007/978-1-4939-8907-2.

Lee, T. (1994). Building skeleton models via 3-D medial surface/Axis thinning algorithms. *Graphical Models and Image Processing, 56*(6), 462–478. https://doi.org/10.1006/gmip.1994.1043

Lucey, J. A., Teo, C. T., Munro, P. A., & Singh, H. (1997). Rheological properties at small (dynamic) and large (yield) deformations of acid gels made from heated milk. *Journal of Dairy Research, 64*(4), 591–600. https://doi.org/10.1017/S0022029997002380

Lucey, J. A., Wilbanks, D. J., & Horne, D. S. (2022). Impact of heat treatment of milk on acid gelation. *International Dairy Journal, 125*, Article 105222. https://doi.org/10.1016/j.idairyj.2021.105222

Marchin, S., Putaux, J. L., Pignon, F., & Léonil, J. (2007). Effects of the environmental factors on the casein micelle structure studied by cryo transmission electron microscopy and small-angle x-ray scattering/ultrasmall-angle x-ray scattering. *Journal of Chemical Physics, 126*(4). https://doi.org/10.1063/1.2409933

Modler, H. W., & Kalab, M. (1983). Microstructure of yogurt stabilized with milk proteins. *Journal of Dairy Science, 66*(3), 430–437. https://doi.org/10.3168/jds.S0022-0302(83)81810-4

Nieuwland, M., Bouwman, W. G., Bennink, M. L., Silletti, E., & de Jongh, H. H. J. (2015). Characterizing length scales that determine the mechanical behavior of gels from crosslinked casein micelles. *Food Biophysics, 10*(4), 416–427. https://doi.org/10.1007/s11483-015-9399-y

Ong, L., Dagastine, R. R., Kentish, S. E., & Gras, S. L. (2010). The effect of milk processing on the microstructure of the milk fat globule and rennet induced gel observed using confocal laser scanning microscopy. *Journal of Food Science, 75*(3). https://doi.org/10.1111/j.1750-3841.2010.01517.x

Post, A. E., Arnold, B., Weiss, J., & Hinrichs, J. (2012). Effect of temperature and pH on the solubility of caseins: Environmental influences on the dissociation of αS-and β-casein. *Journal of Dairy Science*, 1603–1616. https://doi.org/10.3168/jds.2011-4641

Pujals, S., Feiner-Gracia, N., Delcanale, P., Voets, I., & Albertazzi, L. (2019). Super-resolution microscopy as a powerful tool to study complex synthetic materials. *Nature Reviews Chemistry*. https://doi.org/10.1038/s41570-018-0070-2

Reitmaier, M., Barbosa, B., Sigler, S., Heidebrecht, H., & Kulozik, U. (2020). Impact of different aqueous phases on casein micelles : Kinetics of physicochemical changes under variation of water hardness and dia fi ltration conditions. *International Dairy Journal, 109*, Article 104776. https://doi.org/10.1016/j.idairyj.2020.104776

Rust, M. J., Bates, M., & Zhuang, X. (2006). Sub-diffraction-limit imaging by stochastic optical reconstruction microscopy (STORM). *Nature Methods, 3*(10), 793–795. https://doi.org/10.1038/nmeth929

Schneider, C. A., Rasband, W. S., & Eliceiri, K. W. (2012). NIH image to ImageJ: 25 years of image analysis. *Nature Methods, 9*(7), 671–675. https://doi.org/10.1038/nmeth.2089

Sharma, S. K., & Dalgleish, D. G. (1993). Interactions between milk serum proteins and synthetic fat globule membrane during heating of homogenized whole milk. *Journal of Agricultural and Food Chemistry, 41*(9), 1407–1412. https://doi.org/10.1021/jf00033a011

Singh, H., Roberts, M. S., Munro, P. A., & Teo, C. T. (1996). Acid-induced dissociation of casein micelles in milk: Effects of heat treatment. *Journal of Dairy Science, 79*(8), 1340–1346. https://doi.org/10.3168/jds.S0022-0302(96)76490-1

Sone, I., Hosoi, M., Geonzon, L. C., Jung, H., & Bernadette, F. (2022). Gelation and network structure of acidified milk gel investigated at different length scales with and without addition of iota -carrageenan. *Food Hydrocolloids, 123*(September 2021), Article 107170. https://doi.org/10.1016/j.foodhyd.2021.107170

Walstra, P. (1990). On the stability of casein micelles. *Journal of Dairy Science, 73*(8), 1965–1979. https://doi.org/10.3168/jds.S0022-0302(90)78875-3